Landscape Ecol
https://doi.org/10.1007/s10980-020-01022-8

RESEARCH ARTICLE

# Spatiotemporal variations of albedo in managed agricultural landscapes: inferences to global warming impacts (GWI)

**Pietro Sciusco · Jiquan Chen · Michael Abraha · Cheyenne Lei · G. Philip Robertson · Raffaele Lafortezza · Gabriela Shirkey · Zutao Ouyang · Rong Zhang · Ranjeet John**

Received: 25 October 2019 / Accepted: 26 April 2020


**Abstract**

*Context* Albedo can be used to quantify ecosystem and landscape contributions to local and global climate. Such contributions are conventionally expressed as radiative forcing (RF) and global warming impact (GWI). We contextualize our results within landscape carbon production and storage to highlight the importance of changes in albedo for landscape GWI from multiple causes, including net ecosystem production (NEP) and greenhouse gas (GHG) emissions.

*Objective* To examine the spatiotemporal changes in albedo ($\Delta\alpha$) in contrasting managed landscapes through calculations of albedo-induced RF ($RF_{\Delta\alpha}$) and GWI ($GWI_{\Delta\alpha}$) under different climatic conditions.

*Methods* We selected five contrasting landscapes within the Kalamazoo River watershed in southern Michigan USA as proof of concept. The daily MCD43A3 MODIS (V006) product was used to analyze the inter- and intra-annual variations of growing season albedo. In addition, the variations of $RF_{\Delta\alpha}$ and $GWI_{\Delta\alpha}$ were computed based on landscape composition and climate.

**Electronic supplementary material** The online version of this article (https://doi.org/10.1007/s10980-020-01022-8) contains supplementary material, which is available to authorized users.

P. Sciusco (✉) · J. Chen · C. Lei · G. Shirkey
Department of Geography, Environment & Spatial Sciences, Michigan State University, East Lansing, MI 48823, USA
e-mail: sciuscop@msu.edu

P. Sciusco · J. Chen · M. Abraha · C. Lei · R. Lafortezza · G. Shirkey
Center for Global Change and Earth Observations, Michigan State University, East Lansing, MI 48823, USA

M. Abraha · G. P. Robertson
Great Lakes Bioenergy Research Center, Michigan State University, East Lansing, MI 48824, USA

M. Abraha · G. P. Robertson
W.K. Kellogg Biological Station, Michigan State University, Hickory Corners, MI 49060, USA

R. Lafortezza
Department of Agricultural and Environmental Sciences, University of Bari "A. Moro", 70126 Bari, Italy

R. Lafortezza
Department of Geography, The University of Hong Kong, Centennial Campus, Pokfulam Road, Hong Kong, China

Z. Ouyang
Department of Earth System Science, Stanford University, Stanford, CA 94305, USA

R. Zhang
Zhejiang Tiantong Forest Ecosystem National Observation and Research Station, School of Ecological and Environmental Sciences, East China Normal University, Shanghai 200241, China

Published online: 06 May 2020

*Results* The $RF_{\Delta\alpha}$ ($-$ 5.6 W $m^{-2}$) and $GWI_{\Delta\alpha}$ ($-$ 1.3 $CO_{2eq}$ $ha^{-1}$ $year^{-1}$) were high in forest-dominated landscapes, indicating cooling effects and $CO_{2eq}$ mitigation impacts similar to crops. The $CO_{2eq}$ mitigation of cropland-dominated landscapes was on average 52% stronger than forest-dominated landscapes. In the landscape with the highest proportion of forest, under dry and wet conditions $CO_{2eq}$ mitigation was reduced by up to 24% and $\sim$ 30%, respectively; in one cropland-dominated landscape wet conditions reduced $CO_{2eq}$ mitigation by 23%.

*Conclusions* Findings demonstrate that quantifying spatiotemporal changes in albedo in managed landscapes and under different climatic conditions is essential to understand how landscape modification affects $RF_{\Delta\alpha}$ and $GWI_{\Delta\alpha}$ and thereby contributes to ecosystem-level GWI.

**Keywords** Albedo · Land mosaics · Radiative forcing · Global warming impact · Cropland · Forest

## Introduction

Decoupling the causes and consequences of ecosystem functions and services at multiple spatial scales represents an important scientific frontier in landscape ecology (Raudsepp-Hearne et al. 2010; Antón et al. 2011; Chen et al. 2013; Yuan and Chen 2015; Seidl et al. 2016). Land use and land cover change (LULCC) caused by human activities (e.g., land use), natural disturbances (e.g., wildfires) and global warming directly affects regional and global climate through the exchange of energy, carbon, water, and greenhouse gases (GHGs) between the land surface and the atmosphere (Bright et al. 2015; Bonan 2016). Management activities and disturbances such as cultivation, burning, and grazing not only influence GHG emissions but also alter the surface radiation balance (Pielke et al. 2011; Shao et al. 2014). Unfortunately, little effort has been directed towards investigating resulting changes in surface radiation balance (e.g., changes in albedo) at landscape scales (Euskirchen et al. 2002; Chen et al. 2004).

Albedo—the ratio of solar radiation reflected by a surface to the total incoming solar radiation (e.g., surface radiation balance)—is a measurable physical variable that can be used to quantify ecosystem and landscape contributions to local and global climate (Dickinson 1983; Picard et al. 2012; Brovkin et al. 2013; Li et al. 2016; Storelvmo et al. 2016). Changing albedo has been proposed as one of several geoengineering options for climate change mitigation (Lenton and Vaughan 2009; Goosse 2015) and albedo is also important for understanding exchanges of energy and mass between terrestrial surfaces and the atmosphere (Merlin 2013). Albedo is in its early stages of incorporation into climate models, but it is useful for deriving different mechanisms to lower climate warming by potentially increasing the reflectance of energy back into the atmosphere (Lenton and Vaughan 2009). Although LULCC (e.g., conversions from forest to biofuel, grassland, and cropland) can significantly alter albedo (Bala et al. 2007; Cai et al. 2016), the magnitude of changes depends on vegetation type and canopy structure (see also Bennett et al. 2006; Tian et al. 2018).

Albedo is also highly correlated with leaf wetness, soil moisture, and soil water content (Henderson-Sellers and Wilson 1983; Wang et al. 2004)—which are strongly related to precipitation and its temporal distribution—and as well with plant phenology and vegetation structure (Luyssaert et al. 2014), plant or tree height (Betts 2001), and agricultural practices (Houspanossian et al. 2017)—this last scarcely considered (Zhang et al. 2013; Jeong et al. 2014). For example, Culf et al. (1995) reported decreased albedo in forests as a function of darker leaves and darker soils under wet conditions. Berbet and Costa (2003) found that ranchlands were characterized by variable albedo throughout the entire year depending on climatic conditions (e.g., dry vs wet periods), whereas forests were characterized by higher and lower albedo in both dry and wet periods, respectively.

Changes in atmospheric conditions and land mosaics due to LULCC can affect the Earth's radiation balance (Gray 2007). Radiative forcing (RF) has been widely used to describe this imbalance as changes in the fraction of solar energy reflected by the Earth's surface (Mira et al. 2015), whether anthropogenic or

R. Zhang
Center for Global Change and Ecological Forecasting, East China Normal University, Shanghai 200062, China

R. John
Department of Biology, University of South Dakota, Vermillion, SD 57069, USA

natural (Lenton and Vaughan 2009). RF can thus be used to compare modifications in radiation balance due to atmospheric/surface albedo changes or due to GHG emissions. Previous studies (Betts 2000; Akbari et al. 2009) have developed methodologies to relate RF to $CO_{2eq}$, used to calculate ecosystem-scale contributions to global warming impacts (GWIs)—a common measure for quantifying RFs of different GHGs and other agents (Fuglestvedt et al. 2003; Forster et al. 2007; Peters et al. 2011). GWI allows us to directly relate anthropogenic activities to GHG emissions (Haines 2003; Davin et al. 2007; Cherubini et al. 2012; Robertson et al. 2017) and to understand and quantify the impact of an ecosystem on climate.

Despite escalating efforts to examine the magnitude and dynamics of albedo change due to LULCC, previous studies have focused on albedo, RF, and GWI differences among the cover types within landscapes or regions (Haas et al. 2001; Román et al. 2009; Carrer et al. 2018; Chen et al. 2019). For example, previous studies have shown that deforestation and expanding agricultural lands have played an important role in surface cooling of the northern hemisphere due to increased surface albedo and regeneration of forests after harvesting (Betts 2001; Govindasamy et al. 2001; Lee et al. 2011). Georgescu et al. (2011) simulated strong cooling effects—equivalent to a reduction in carbon emission of 78 t C $ha^{-1}$—by increasing the surface albedo of agricultural lands across the central United States. Loarie et al. (2011) demonstrated that introducing sugar cane production into cropland/pasture landscapes of Brazil increased albedo and evapotranspiration, which in turn appeared to cool the local climate. Importantly, to quantify the contribution of LULCC to global warming/cooling, GWI should be computed with reference to albedo due to pre-existing conditions (i.e., $\Delta\alpha$).

Here we examine the spatiotemporal changes of albedo in contrasting managed landscapes as compared to pre-existing forests through calculations of albedo-induced RF ($\Delta RF_{\Delta\alpha}$) and GWI ($\Delta GWI_{\Delta\alpha}$) under different precipitation regimes (i.e., climatic conditions). We express the relationship between landscape albedo and $GWI_{\Delta\alpha}$ (Fig. 1) as:

$$[\Delta\alpha_i \times \Delta area_l \times \Delta c\lim ate_l] \rightarrow \Delta RF_{\Delta\alpha} \rightarrow \Delta GWI_{\Delta\alpha} \quad (1)$$

where $\Delta GWI_{\Delta\alpha}$ is net landscape albedo-induced GWI, $\Delta\alpha_i$ is the difference between mean albedo at a cover type $i$ and mean forest albedo (i.e., the reference), $\Delta area_l$ is variation of cover-type proportion for landscape $l$, and $\Delta climate_l$ is the variation of climatic conditions for landscape $l$. More specifically, we aim to estimate the magnitude and seasonal changes in albedo so that $\Delta GWI_{\Delta\alpha}$ can be assessed at ecosystem, landscape, and watershed scales, and included in ecosystem GWI assessments (e.g., Gelfand and Robertson 2015). We further contextualize our results within landscape carbon production and storage to highlight the importance of changes in landscape $GWI_{\Delta\alpha}$ from multiple causes, including net ecosystem production (NEP) and GHG emissions. The framework developed in this study (Eq. 1, Fig. 1) can be applied to any landscape to for compute landscape $GWI_{\Delta\alpha}$. To this end, we selected five contrasting landscapes in the Kalamazoo River watershed of southwestern Michigan U.S.A. as a proof of concept to investigate inter- and intra-annual variations of albedo under three different climatic conditions.

## Materials and methods

### Study area

We chose five contrasting landscapes (Fig. 2) in the Kalamazoo River watershed, located in southwest Michigan, USA, for proof of concept. Within the 526,100 ha watershed, the long-term mean annual temperature is 9.9 °C and the average annual precipitation is 900 mm that is evenly distributed throughout the year (Michigan State Climatologist's Office 2013). The watershed includes portions of 10 counties: Allegan, Ottawa, Van Buren, Kent, Barry, Kalamazoo, Calhoun, Eaton, Jackson, and Hillsdale. Prior to European settlement, the watershed was dominated by forests (Brown et al. 2000) with interspersed tallgrass prairies, savannas, lakes, wetlands, and oak openings (Chapman and Brewer 2008). The watershed however has undergone significant LULCC since then. Present-day forest areas are secondary successional forests that followed their complete harvest by European settlers in the late 1800 s (Brown et al. 2000). Today, the watershed consists of cultivated crops, deciduous forest stands, pasture-hay grasslands,

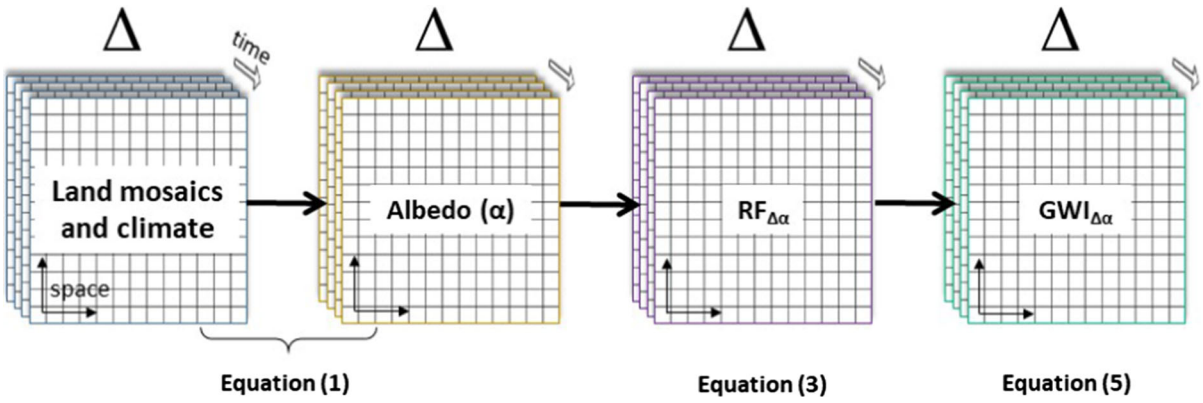


**Fig. 1** Schematic diagram showing the relationship between landscape albedo and $GWI_{\Delta\alpha}$

inland lakes, wooded wetlands, and urban areas. Dominant soils of the watershed are Alfisols of medium to coarse texture that allows a continuous recharge of groundwater (Schaetzl et al. 2009).

We randomly selected five 10,000 ha landscapes (Fig. 2) (Burton et al. 1998) that represent the main ecoregions of the watershed, i.e., areas characterized by similar vegetation, with the same type, quality and quantity of environmental resources (Omernik and Griffith 2014). The Kalamazoo River watershed includes three U.S. EPA ecoregions: Eastern Temperate Forest (Level I), Mixed Wood Plain (Level II), and Southern Michigan/Northern Indiana Drift Plain (Level III). At a finer scale, five Level IV ecoregions (Table S1) exist in the watershed: Battle Creek Outwash Plain (56b), Michigan Lake Plain (56d), Lake Michigan Moraines (56f), Lansing Loamy Plain (56 g), and Interlobate Dead Ice Moraines (56 h). (https://www.epa.gov/eco-research/ecoregion-download-files-state-region-5#pane-20). We used the five landscapes to represent the five Level IV ecoregions so that each landscape fell within an individual Level IV ecoregion.

Each landscape has different proportions of urban, cropland, barren, forest, water, wetland, and grassland cover types (Table 1). Two of the five landscapes have a higher proportion of forest ($FOR_1$ highest proportion of forest, and $FOR_2$ s highest proportion); while the remaining three landscapes are dominated by cropland ($CROP_1$, $CROP_2$, and $CROP_3$, from high to low proportion of cropland, respectively) (Table 1). Given that forest was the dominant land cover type prior to European settlement within each landscape (Brown et al. 2000), we considered the average albedo of all forest portions within each of the five landscapes during the growing season at 10:30 a.m. local time (UTC) as the reference albedo (e.g., MODIS Terra morning overpass time). Thereafter, in each landscape, changes in albedo ($\Delta\alpha$) were obtained by calculating the difference between mean cropland and mean forest albedos, and then used to calculate $RF_{\Delta\alpha}$ and $GWI_{\Delta\alpha}$.

### Landscape structure

The landscape structure of the watershed was quantified from a classified land cover map for 2011 (Fig. 2) at 30 × 30 m spatial resolution, which was produced using the Landsat archives from the USGS Earth Explorer/GLOVIS portals (https://earthexplorer.usgs.gov/). The land cover map was obtained following the Anderson level I classification scheme and included seven land cover types: (1) urban, (2) cropland, (3) barren, (4) forest, (5) water, (6) wetland, and (7) grassland. The details of the accuracy assessment (i.e., producer and user's accuracy for each class type and the overall accuracy in an error matrix) of the classification were provided in Chen et al. (2019).

### MODIS Albedo

Albedo datasets were obtained from the most recent collection (V006) of the MCD43A3 MODIS Bidirectional Reflectance Distribution Function (BRDF) product (https://doi.org/10.5067/MODIS/MCD43A3.006). MOD43A3 is a daily product at 500 × 500 m spatial resolution obtained by inversion of a

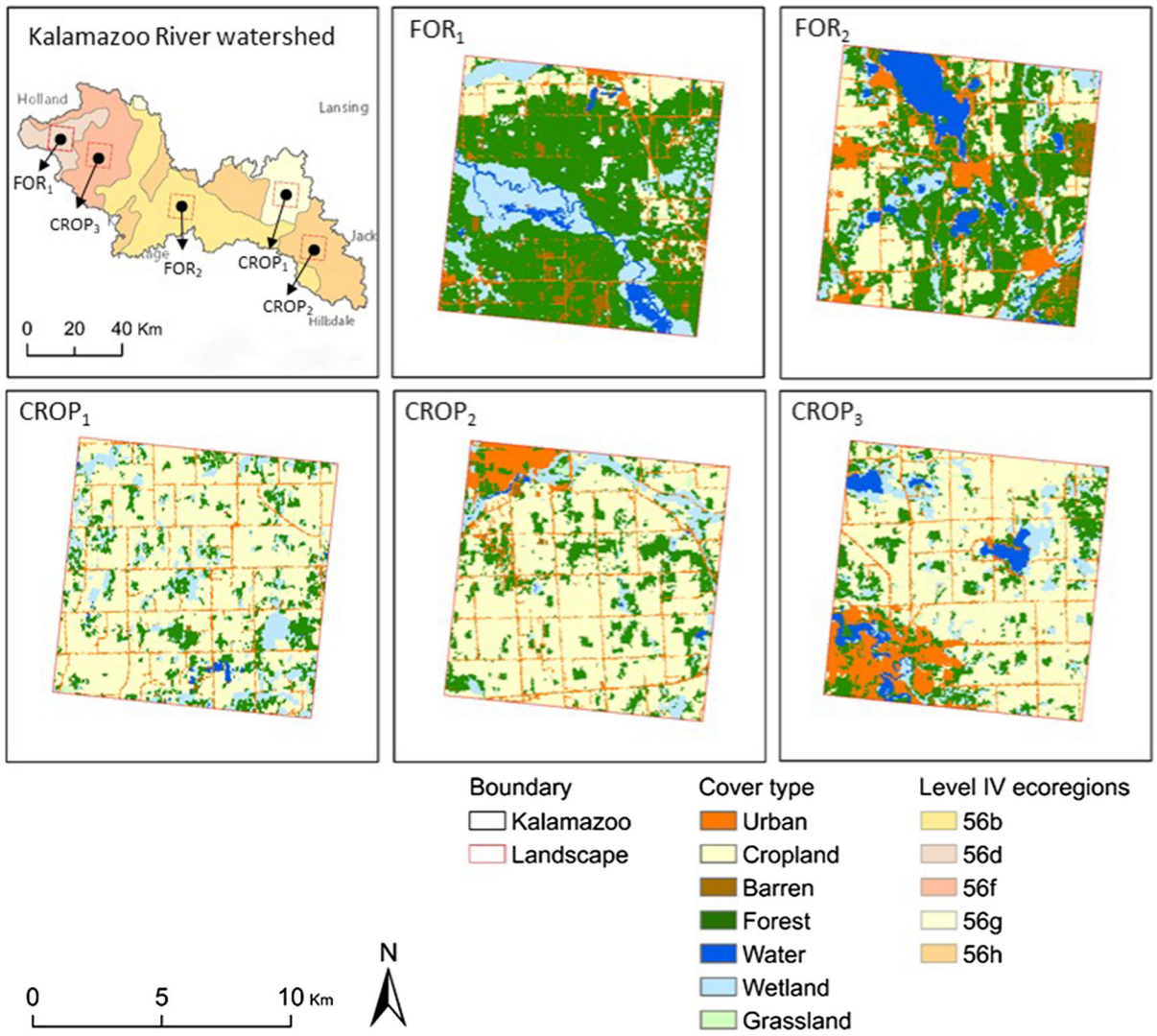


**Fig. 2** Locations of the five landscapes ($FOR_1$, $FOR_2$, $CROP_1$, $CROP_2$, $CROP_3$) within the Kalamazoo River watershed in the southwest Michigan (USA). Each landscape falls within a unique Level IV ecoregion defined by the United States Environmental Protection Agency (US EPA). Basemap sources: *Esri, HERE, Garmin, USGS, Intermap, INCREMENT P, NRCAN, Esri Japan, METI, Esri China (Hong Kong), NOSTRA, © OpenStreetMap contributors, and the GIS User Community*

Bidirectional Reflectance Distribution Function (the BRDF) model against a 16-day moving window of MODIS observations. The BRDF model was then used to derive the black-sky (associated to direct solar radiation) and white-sky (associated to diffuse radiation) albedos (Wang et al. 2014). We only considered snow-free, white-sky albedo at a shortwave length of 0.3-5.0 µm (hereafter, $\alpha_{SHO}$ and expressed in percentage). For each image, the "Albedo_WSA_shortwave" (white-sky albedo) band was selected and rescaled to 0-1. Only high-quality data were selected within the "full BRDF inversion" quality band (QA = 0). The "Snow_BRDF_Albedo" band in the MCD43A2 product was used to filter and exclude pixels with snow albedo retrievals (Chrysoulakis et al. 2018).

### Modis ndvi

Previous studies (e.g., Campbell and Norman 1998; Bonan 2008; Iqbal 2012; Liang et al. 2013; Zhao and Jackson 2014; Bright et al. 2015; Kaye and Quemada 2017; Sun et al. 2017) have thoroughly addressed the importance of snow cover on variability/uncertainty of albedo. Here, we focused on albedo change, $RF_{\Delta\alpha}$ and $GWI_{\Delta\alpha}$ only during the growing season when maximum variability of watershed crop phenology can be related with changes in climatic conditions and human disturbances at the landscape level. Therefore, for each year, we identified the "growing season" during March–October by detecting the greenness onset/offset for the entire Kalamazoo River watershed. To do so, for each year, we used a 16-day composite time series of the normalized difference vegetation index (NDVI) to detect the inflection points (i.e., dates) when the maximum and minimum change rate of NDVI occurred (Jeong et al. 2011). We obtained NDVI at a 250 × 250 m spatial resolution from the most recent collection (V006) of the MYD13Q1 MODIS product (https://doi.org/10.5067/MODIS/MYD13Q1.006). Finally, we divided each growing season (March–October) into three periods (hereafter, seasons)—spring, summer, and fall using astronomical season (e.g., spring equinox, summer solstice, and fall equinox).

### Precipitation data

Daily precipitation data at a 4 × 4 km spatial resolution were obtained from the Parameter-elevation Regressions on Independent Slopes Model group (PRISM) AN81d product (http://www.prism.oregonstate.edu/) over the 2012–2017 time period. We also calculated the cumulative precipitation of the five landscapes during the growing season from March through October. For the time period considered (e.g., 2012–2017), we then identified three years as dry, normal and wet years: 2012, 2017 and 2016, respectively. The Midwest of U.S.A. experienced 6 weeks of summer drought during June-July in 2012 (Mallya et al. 2013), resulting in a growing season precipitation of $< 490$ mm. In 2017, the watershed received over 750 mm, while this was $\sim$ 700 mm (i.e., near average) for 2017. All analysis and processing of albedo, NDVI, and precipitation data were performed on the Google Earth Engine (GEE) platform (Gorelick et al. 2017), where the MODIS products were uploaded, filtered to the date of interest, and clipped to the shape file for each of the five landscapes.

### Statistical analysis

We performed analysis of variance (ANOVA) to examine the change in albedo with land cover type and landscape structure within the three-year study period and across three seasons. The following linear model was applied:

$$\alpha_{SHO} = landscape \times cover\,type \times year \times seasons \quad (2)$$

where $\alpha_{SHO}$ is the snow-free white-sky albedo at the shortwave length at a daily step acquired from MODIS at 10:30 a.m. local time (UTC); landscape, cover type, year, and season are the five landscapes ($FOR_1$, $FOR_2$, $CROP_1$, $CROP_2$, $CROP_3$), the seven cover types (Table 1) at each landscape, the three years (dry, wet, and normal), and the three astronomical seasons

**Table 1** Land cover composition of the five landscapes

| Cover type | Landscape (ha (%)) | | | | |
|---|---|---|---|---|---|
| | $FOR_1$ | $FOR_2$ | $CROP_1$ | $CROP_2$ | $CROP_3$ |
| Urban | 513 (5.2) | 1330 (13.3) | 545 (5.5) | 1047 (10.5) | 1341 (13.4) |
| Cropland | 1035 (10.5) | 2597 (26.0) | **6807 (68.1)** | **6442 (64.5)** | **5713 (57.2)** |
| Barren | 530 (5.4) | 286 (2.9) | 49 (0.5) | 62 (0.6) | 64 (0.6) |
| Forest | **5672 (57.5)** | **3833 (38.4)** | 1415 (14.2) | 1670 (16.7) | 1477 (14.8) |
| Water | 410 (4.2) | 922 (9.2) | 56 (0.6) | 43 (0.4) | 442 (4.4) |
| Wetland | 1669 (16.9) | 1012 (10.1) | 1101 (11.0) | 693 (6.9) | 917 (9.2) |
| Grassland | 30 (0.3) | 12 (0.1) | 21 (0.2) | 35 (0.4) | 38 (0.4) |

Bold values indicate the cover type dominating the landscape

(spring, summer, and fall), respectively. We also considered the interaction terms among the independent variables in our ANOVA.

To test the normality of our data we checked the distribution of the residuals. We then carried out ANOVA and Tukey tests for multiple comparisons using the R-package 'lsmeans' (R Core Team 2017).

### Radiative forcing (RF) and global warming impact (GWI)

To quantify the potential of RF caused by changes in albedo, we referred to the direct albedo-induced RF at the top-of-atmosphere ($RF_{\Delta\alpha}$), where $\Delta\alpha$ is the change of $\alpha_{SHO}$ (i.e., the absolute difference between mean cropland and mean forest albedos in each of the five landscapes). We calculated $RF_{\Delta\alpha}$ (W $m^{-2}$) following the algorithms of Carrer et al. (2018):

$$RF_{\Delta\alpha}(t) = -\frac{1}{N}\sum_{d=1}^{N} SW_{in} T_a \Delta\alpha \quad (3)$$

where $RF_{\Delta\alpha}$ is the mean albedo-induced radiative forcing at the top-of-atmosphere over the growing season (t), $N$ is the number of days in the growing season, $SW_{in}$ is the incoming solar radiation at the surface, $T_a$ is the upward atmospheric transmittance and $\Delta$ is the albedo difference (i.e., between mean cropland and mean forest albedos). By multiplying both $SW_{in}$ and $\Delta$ by $T_a$, we calculated the instantaneous amount of radiation that leaves the atmosphere at 10:30 a.m. UTC. It is worth reiterating that all the variables (i.e., $SW_{in}$, $\Delta\alpha$, and $T_a$) refer to the specific time of 10:30 a.m. UTC (e.g., MODIS Terra morning overpass time) and were considered to represent daily means. Negative values of $RF_{\Delta\alpha}$ indicate a cooling effect due to the differences between mean cropland and mean forest albedos.

While previous studies (e.g., Lenton and Vaughan 2009; Cherubini et al. 2012) used a global annual average value of 0.854 for $T_a$, we calculated $T_a$ as the ratio of incoming solar radiation at the top of the atmosphere ($SW_{TOA}$) to that at the surface ($SW_{in}$) at 10:30 a.m. UTC. By assuming a same value of upward and downward atmospheric transmittances (Carrer et al. 2018), $SW_{in}$ (W $m^{-2}$) was obtained from a local eddy covariance (EC) tower located at the Kellogg Biological Station Long-term Ecological Research site (42° 24′ N, 85° 24′ W) (Abraha et al. 2015), while $SW_{TOA}$ (W $m^{-2}$) was calculated as:

$$SW_{TOA} = S_{po}\cos(\theta)d \quad (4)$$

where $S_{po}$ is the solar constant (1360 W $m^{-2}$), $\cos(\theta)$ is the cosine of the solar zenith angle, obtained from the MCD43A2 (V006) MODIS BRDF Albedo Quality product (https://doi.org/10.5067/MODIS/MCD43A2.006), applying the "BRDF_Albedo_LocalSolarNoon" band, and $d$ is the mean Earth-Sun distance. We then converted RF into the $CO_2$ equivalent ($CO_{2eq}$) by using the GWI algorithms of Bird et al. (2008) and Carrer et al. (2018):

$$GWI_{\Delta\alpha}(t) = \frac{SRF_{\Delta\alpha(t)}}{AFrf_{CO_2}}\frac{1}{TH} \quad (5)$$

where $GWI_{\Delta\alpha}$ is the $CO_{2eq}$ (kg $CO_{2eq}$ $m^{-2}$ $year^{-1}$) GWI due to $\Delta\alpha$, represented by MODIS $\alpha_{SHO}$ acquisitions at 10:30 a.m. UTC, i.e., assuming that the values represent the mean $CO_{2eq}$ mitigation impact of each landscape during the growing season March–October ($t$), $RF_{\Delta\alpha}$ is the mean RF due to $\Delta\alpha$ over the growing season March–October ($t$) (Eq. 3), $S$ is cropland area (ha) for which we hypothesized the change of albedo occurred, $AF$ is the $CO_2$ airborne fraction (0.48, Muñoz et al. 2010) obtained from the exponential $CO_2$ decay function (see Bird et al. 2008 for more details), and $TH$ is the time horizon of potential global warming fixed at 100 years (Kaye and Quemada 2017). Lastly, the parameter $rf_{CO_2}$—the marginal RF of $CO_2$ emissions at the current atmospheric concentration—is kept as a constant (Muñoz et al. 2010; Bright et al. 2015; Carrer et al. 2018) at 0.908 W kg $CO_2^{-1}$.

Negative values of $GWI_{\Delta\alpha}$ indicate $CO_{2eq}$ mitigation. We calculated the annual $GWI_{\Delta\alpha}$ as 1/100 of the total $CO_{2eq}$ to normalize to the 100 year time horizon used in the Kyoto Protocol (Boucher et al. 2009). Notably, here we assumed that the same land mosaic in each landscape will be maintained for the duration of 100 years. Previous studies (Betts 2000; Akbari et al. 2009) have also used a constant AF as opposed to the exponential $CO_2$ decay function; however, the computed GWIs are similar (Bright 2015).

## Results

Two of the five landscapes ($FOR_1$ and $FOR_2$) were dominated by forests (Table 1), with a forest coverage of 57.5% in $FOR_1$ and 38.4% in $FOR_2$. Wetlands and croplands accounted for 16.9% and 10.5% of landscape, respectively, in $FOR_1$ (Table 1), but only 10.1% and 26% in $FOR_2$ where urban land was also the highest (13.3%). Croplands were dominant in $CROP_1$, $CROP_2$, and $CROP_3$ (Table 1), with 68.1%, 64.5%, and 57.2% of area coverage, respectively. Forest cover ranked the second highest in these landscapes (14.2%, 16.7%, and 14.8%, respectively). Bare soils, grasslands, and water accounted for small portions of all five landscapes.

The entire watershed had an $\alpha_{SHO}$ of 15.9% during the dry (2012) and wet (2016) years and of 15.6% during the normal (2017) year (Table S2), yielding an overall average of 15.8% with a low inter-annual variation. Each cover type contributed differently to $\alpha_{SHO}$ at the watershed level. In particular, croplands and water bodies showed the highest (16.6%) and lowest (12.1%) $\alpha_{SHO}$, respectively, with the highest values occurring in both 2012 (16.6% $\pm$ 1.0) and 2016 (16.6% $\pm$ 1.1) for croplands, and the lowest in 2017 (11.9% $\pm$ 3.4) for water. The other cover types showed similar $\alpha_{SHO}$ values, ranging 15.1–15.6% for barren and grassland, 15.2% for urban and forests and 15.4% for wetlands. At the landscape level, $\alpha_{SHO}$ of forest, which was considered as reference, was generally lower than that of croplands. In particular, $FOR_1$ and $FOR_2$ averaged a low $\alpha_{SHO}$ of 14.6% and 13.9%, respectively, whereas $CROP_1$, $CROP_2$, and $CROP_3$ recorded higher values of 16.7%, 16.4%, and 16.2%, respectively. However, $FOR_1$ and $FOR_2$ demonstrated the highest $\alpha_{SHO}$ in 2012 (14.7% $\pm$ 0.8 and 14.1% $\pm$ 2.3, respectively), while $CROP_1$, $CROP_2$, and $CROP_3$ demonstrated the highest $\alpha_{SHO}$ in different years, such as 2016 for $CROP_1$ (17.0% $\pm$ 0.8), 2012 and 2016 for $CROP_2$ (16.5% $\pm$ 0.6), and 2017 for $CROP_3$ (16.3% $\pm$ 1.7). In the forest-dominated landscapes, all cover types showed higher $\alpha_{SHO}$ during the dry year (2012). However, for $FOR_2$, $\alpha_{SHO}$ values of cropland and barren were high in the wet year (2016). In the cropland-dominated landscapes, the highest $\alpha_{SHO}$ value (17.1%) was observed in $CROP_3$ ($\pm$ 1.1) for croplands in 2017, and in $CROP_1$ for both urban ($\pm$ 0.6) and croplands ($\pm$ 0.8) in 2016.

Our ANOVA model ($R^2 = 0.64$) (Table 2) indicated that the variation of $\alpha_{SHO}$ was significant ($p$ value $< 0.001$) among the five landscapes (i.e., ecoregions) ($\omega^2 = 26.6\%$) by cover type (i.e., landscape mosaics) ($\omega^2 = 11.1\%$) and their interactions ($\omega^2 = 5.2\%$), with year and its interactions explaining $< 1\%$ of the variation. However, the variation from season (i.e., seasonality) ($\omega^2 = 15.9\%$) explained more than cover type.

Forest-dominated landscapes ($FOR_1$ and $FOR_2$) showed lower least square means (LSM) of $\alpha_{SHO}$ ($LSM\alpha_{SHO}$) than cropland-dominated landscapes ($CROP_1$, $CROP_2$ and $CROP_3$) (Fig. 3a) over the three years. A decreasing inter-annual trend (between 2012, 2016, and 2017 growing seasons) characterized $FOR_1$, $FOR_2$, and $CROP_2$, with $FOR_1$ showing statistically higher $LSM\alpha_{SHO}$ in the dry (2012) year; whereas $CROP_2$ showed statistically lower $LSM\alpha_{SHO}$ in the normal (2017) year. In addition, differences in LSM between cropland and forest albedos ($LSM_{\Delta\alpha}$) appeared to be higher in $FOR_1$, $FOR_2$, and $CROP_3$ (Fig. 3b), but with increasing inter-annual trends, than in $CROP_1$ and $CROP_2$. However, only $FOR_2$ showed statistically lower $LSM_{\Delta\alpha}$ in the dry year (2012) (Fig. 3b).

Clear seasonal patterns existed in $\alpha_{SHO}$ and were generally lower in spring and autumn than in the summer (Fig. 4). However, in $CROP_2$, the $\alpha_{SHO}$ of the major cover types (i.e., cropland, forest, urban, and wetland) was the highest in the spring of the dry year. The $\alpha_{SHO}$ of cropland and urban areas in 2017 (a normal year) was also relatively higher in both spring and summer (Fig. $4c_1$–$c_3$). The inter-annual variability between the wet and normal years (Fig. $4b_1$–$b_4$ and $c_1$–$c_4$, respectively) appeared similar, with small differences between $FOR_1$ and $FOR_2$ (e.g., the lowest $\alpha_{SHO}$ occurring in spring in $FOR_1$ and in autumn in $FOR_2$).

The mean $\Delta\alpha$ ranged between 0.4% and 2% (i.e., $\sim$ 1.2% mean difference between mean cropland and mean forest albedos) (Fig. 4$\Delta$a–$\Delta$c); however, the intra-annual variability of $\Delta\alpha$ differed by landscape and year. We found that forest-dominated landscapes ($FOR_1$ and $FOR_2$) had higher $\Delta\alpha$ in spring each year, with the minimum in autumn ($FOR_1$) and summer ($FOR_2$) of every year. Cropland-dominated landscapes ($CROP_1$, $CROP_2$ and $CROP_3CROP_3$) showed higher $\Delta\alpha$ in spring that was more pronounced in 2016 for $CROP_1$ (Fig. 4$\Delta$b), in 2016 and 2017 for

**Table 2** Statistical results of analysis of variance (ANOVA) based on the linear model in Eq. 1 (dependent variable: $\alpha_{SHO}$)

| Variable | DF | SS | MS | F | p | $\omega^2$ | $R^2$ |
|---|---|---|---|---|---|---|---|
| Landscape | 4 | 1.869 | 0.467 | 3689.660 | *** | 0.266 | |
| Seasons | 2 | 1.118 | 0.559 | 4414.651 | *** | 0.159 | |
| Cover type | 6 | 0.779 | 0.130 | 1024.423 | *** | 0.111 | |
| Landscape × cover type | 24 | 0.371 | 0.015 | 121.891 | *** | 0.052 | |
| Landscape × seasons | 8 | 0.142 | 0.018 | 140.167 | *** | 0.020 | |
| Landscape × cover type × seasons | 48 | 0.079 | 0.002 | 12.962 | *** | 0.011 | |
| Year × seasons | 4 | 0.048 | 0.012 | 94.672 | *** | 0.007 | |
| Cover type × seasons | 12 | 0.030 | 0.003 | 19.844 | *** | 0.004 | |
| Landscape × year | 8 | 0.022 | 0.003 | 21.210 | *** | 0.003 | |
| Landscape × year × seasons | 16 | 0.020 | 0.001 | 9.684 | *** | 0.003 | |
| Year | 2 | 0.013 | 0.007 | 51.367 | *** | 0.002 | |
| Landscape × cover type × year | 48 | 0.015 | 0 | 2.505 | *** | 0.002 | |
| Cover type × year | 12 | 0.002 | 0 | 1.278 | | 0 | |
| Cover type × year × seasons | 24 | 0.003 | 0 | 1.047 | | 0 | |
| Landscape × cover type × year × seasons | 96 | 0.011 | 0 | 0.887 | | 0 | 0.64 |
| Residuals | 19,779 | 2.505 | 0 | | | | |

$\omega^2$ indicates variance in the dependent variable $\alpha_{SHO}$ accounted for by the independent variables landscape, cover type, year, seasons, and their interactions

Significance codes: "***" $p < 0.001$, "**" $p < 0.01$, "*" $p < 0.05$, "." $p < 0.1$, " " $p > 0.1$

$CROP_2$ (Fig. 4Δb–Δc), and in 2012 for $CROP_3$ (Fig. 4Δa). However, $CROP_2$ in 2012 was characterized by a different Δα trend—lower in spring and higher in autumn (Fig. 4Δa). The summer Δα variability among the five landscapes was lower in the dry year (Fig. 4Δa) and higher in the normal year (Fig. 4Δc). Two distinct clusters characterized the summer of the wet year (Fig. 4Δb), with $FOR_1$, $FOR_2$ and $CROP_3$ having an Δα of $\geq$ 1% and $CROP_1$ and $CROP_2$ of $\leq$ 0.5%.

All five landscapes had negative $RF_{\Delta\alpha}$ (Table 3; Fig. 5a). Among the cropland-dominated landscapes, $CROP_1$ and $CROP_2$ had similar lower magnitude $RF_{\Delta\alpha}$ values, with minimum and maximum values in the wet (2016) and normal (2017) years, respectively. In particular, $CROP_2$ had $RF_{\Delta\alpha}$ (W $m^{-2}$) of − 1.2 in 2016 and − 1.9 in 2017, followed by $CROP_1$ (− 1.3 and − 2.0) and $CROP_3$ (− 2.9 and − 3.7). Among the forest-dominated landscapes, $FOR_1$ showed a similar trend, with minimum and maximum magnitude $RF_{\Delta\alpha}$ in 2016 and 2017 (− 3.9 and − 5.6, respectively), while $FOR_2$ had the minimum and maximum magnitude $RF_{\Delta\alpha}$ in the dry (2012) and normal (2017) years (− 2.7 and − 2.9, respectively).

As for $RF_{\Delta\alpha}$, all five landscapes showed negative values of $GWI_{\Delta\alpha}$ (Table 3; Fig. 5b), which had inter- and intra-annual trends similar to $RF_{\Delta\alpha}$ (Fig. 5b). In particular, $CROP_1$ and $CROP_2$ had similar lower magnitude $GWI_{\Delta\alpha}$ (Mg $CO_{2eq}$ $ha^{-1}$ $year^{-1}$) values, with minimum ($CROP_1$ and $CROP_2$: − 0.3) and maximum ($CROP_1$: − 0.5 and $CROP_2$: − 0.4) values in the wet (2016) and normal (2017) years, respectively, followed by $CROP_3$ (− 0.7 and − 0.9, respectively). $FOR_1$ showed a similar trend, with minimum and maximum magnitude $GWI_{\Delta\alpha}$ in 2016 and 2017 (− 0.9 and − 1.3, respectively), with statistically higher $GWI_{\Delta\alpha}$ in 2017, while $FOR_2$ had the minimum and maximum magnitude $GWI_{\Delta\alpha}$ in the dry (2012) and both wet and normal (2016 and 2017) years (− 0.6 and − 0.7, respectively) (Table 3; Fig. 5b).

Taking the normal year (2017) as our baseline, the percentage changes between the normal and dry years (e.g., $diff_{2017–2012}$), and the normal and wet years (e.g., $diff_{2017–2016}$) showed reduced Δα, $RF_{\Delta\alpha}$, and $GWI_{\Delta\alpha}$ values (Table 3). In particular, the decrease in Δα was higher in $FOR_2$, $CROP_1$ $CROP_2$ (28.5%, 9.2%, and 19.4%, respectively) for $diff_{2017–2012}$ and in $CROP_1$ and $CROP_2$ (12.6% and 34.3%, respectively) for

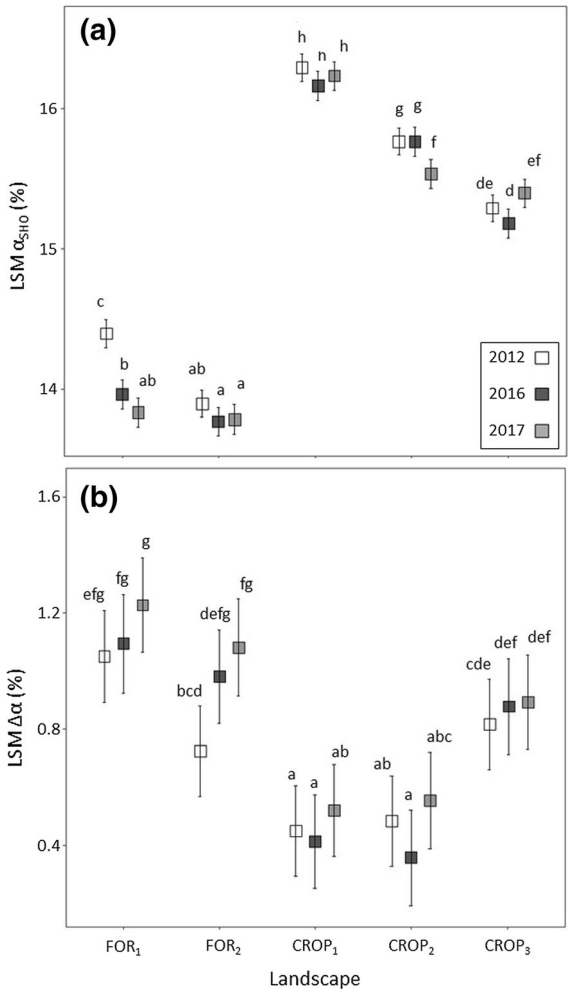


**Fig. 3** Least square means (LSM) multi-comparison analysis of $\alpha_{SHO}$ (**a**) and $\Delta\alpha_{SHO}$ (**b**) in 2012, 2016, and 2017 for each landscape. Boxes indicate the LSM; whiskers represent the lower and upper limits of the 95% family-wise confidence level of the LSM. Boxes sharing the same letters are not significantly different (intra- and inter-annual, as well as within and among the five landscapes) according to the Tukey HSD test

$diff_{2017–2016}$. $FOR_2$ decreased the least from baseline in both $RF_{\Delta\alpha}$ and $GWI_{\Delta\alpha}$ compared to all other landscapes, which had the highest decrease in $diff_{2017–2016}$—$FOR_1$ (29.9%), $CROP_1$ (32.1%), $CROP_2$ (33.4%), and $CROP_3$ (23.3%). Statistically, reductions in $\Delta\alpha$, $RF_{\Delta\alpha}$, and $GWI_{\Delta\alpha}$ values were all significant in $FOR_1$ (for both $diff_{2017–2012}$ and $diff_{2017–2016}$) and in $CROP_2$ (for $diff_{2017–2016}$).

## Discussion

The main finding of our study is that $RF_{\Delta\alpha}$ and $GWI_{\Delta\alpha}$ play an important role in climate change impact due to landscape mosaics. In particular, we found that forests have lower albedo than croplands, which is in consistent with previous studies. In all five landscapes LULCC from forest to cropland showed a cooling effect with negative $RF_{\Delta\alpha}$ and $GWI_{\Delta\alpha}$ values. The results also show that the difference between mean cropland and mean forest albedos during the three years produces on average ~ 64%, 65%, and 28% stronger $CO_{2eq}$ mitigation impacts in the landscape with the highest proportion of forest ($FOR_1$) than in cropland-dominated landscapes ($CROP_1$, $CROP_2$, and $CROP_3$, respectively), presumably due to the lower proportion in cropland (e.g., 10.5% of cropland area) in $FOR_1$. Additionally, dry climatic conditions in 2012 result in the highest albedo in almost all landscapes, although only significantly higher in one of the forest-dominated ($FOR_1$) landscapes, supporting a consensus that dry surfaces reflect more than wet surfaces. Over the growing season, albedo peaks in summer in all cover types, with lower albedo in spring and autumn due to changes in plant phenology.

### Inter- and intra-annual changes in albedo

We compared $\alpha_{SHO}$ values among major cover types (i.e., urban, cropland, forest, and wetland), disregarding those with lower proportions (i.e., grassland, water, and barren) due to their negligible contributions to the total landscape $\alpha_{SHO}$. We observed that croplands and forests had on average 7.8% higher and 0.7% lower albedo than other land covers, respectively. This is in line with previous studies that examined snow-free albedo variations among ecosystems (Jiao et al. 2017; Chen et al. 2019) and across the conterminous United States (Barnes and Roy 2010). Bonan (2008) showed that forests have lower surface albedo than other cover types, contributing to climate warming. Our study indicated that in forest-dominated landscapes ($FOR_1$ and $FOR_2$) the average of inter-annual variation of $\alpha_{SHO}$ was ~ 2.8% lower than that in cropland-dominated landscapes (Table S2; Fig. 3a). Analysis of variance also revealed that the five landscapes (i.e., ecoregions), cover types (i.e., landscape mosaics), and seasons (i.e., seasonality) contributed significantly to the overall variation of $\alpha_{SHO}$.

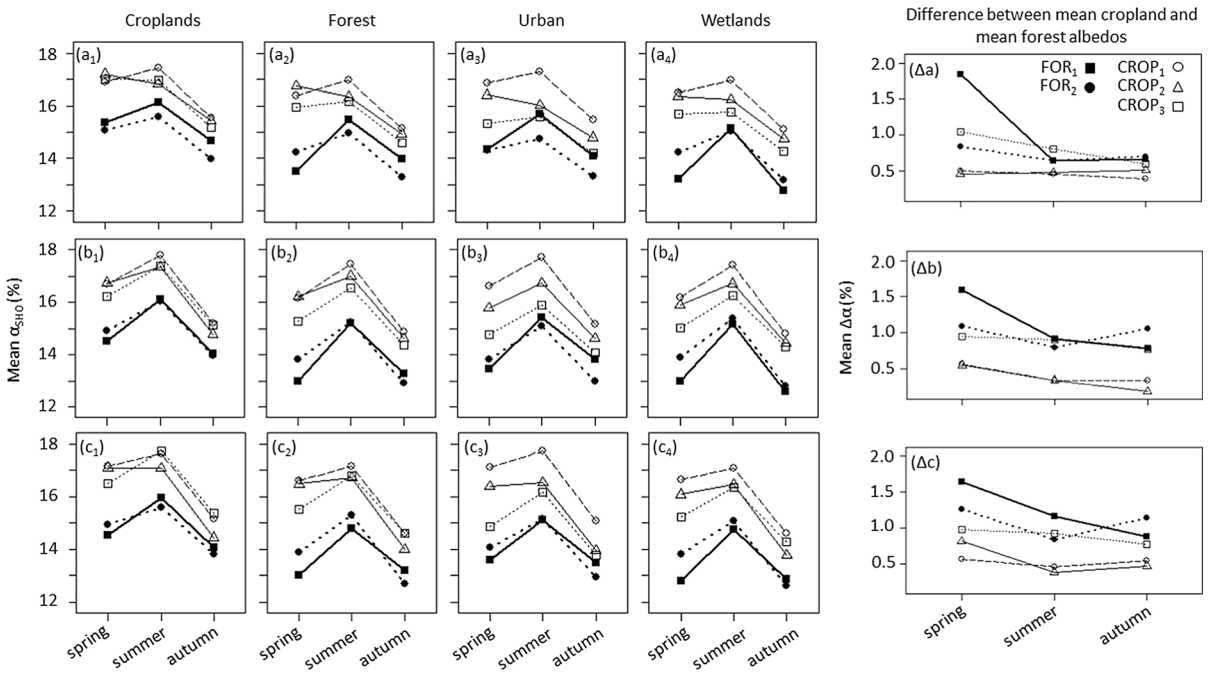


**Fig. 4** Mean $\alpha_{SHO}$ (%) by cover type and season in 2012 ($a_1$–$a_4$), 2016 ($b_1$–$b_4$), and 2017 ($c_1$–$c_4$) for the five landscapes. Mean of the difference between mean cropland and mean forest albedos ($\Delta\alpha_{SHO}$) for the same years (Δa, Δb, and Δc, respectively) is also shown

Specifically, we found that besides the five landscapes, seasons ($\sim$ 16%) contributed by 5% more than cover type (11%) towards variation of $\alpha_{SHO}$ (Table 2).

Changes in $\alpha_{SHO}$ due to LULCC have been widely studied (Chrysoulakis et al. 2018); however, its dynamics at ecosystem-to-landscape scales remain unexplored. For example, Zheng et al. (2019) investigated how vegetation changes affect albedo trends without considering the integrated effect of both cover type and seasonality, while Matthews et al. (2003) investigated the cooling/warming effects of albedo change resulting from deforestation, but failed to consider realistic land cover change scenarios. A number of agricultural management practices are known to mitigate climate change (summarized in Smith et al. 2008; Eagle et al. 2012), including GHG emission reductions and soil carbon storage, but the potential contribution of albedo change as an ecosystem-scale mitigation factor has not been much addressed. For example, tillage practices, harvest timing, residue management, and winter cover crops can all affect surface reflectance in annual cropping systems (Bright et al. 2015; Poeplau and Don 2015; Kaye and Quemada 2017; Robertson et al. 2017) and thus GWI.

To our knowledge, no effort has been made to understand albedo mitigation in terms of both RF and GWI in the context of landscape mosaics characterized by diverse land use type and intensity. Using the framework listed in Eq. 1 and Fig. 1, we were able to integrate spatial (e.g., five landscapes within ecoregions) and temporal (e.g., inter- and intra-annual) changes as main drivers of $\alpha_{SHO}$ variations. Regardless of land composition, cropland-dominated landscapes showed a higher intra-annual variability of $\alpha_{SHO}$ than forests under dry, wet, and normal climatic conditions (Fig. 4a–c), likely due to the higher disturbances that croplands experience (i.e., fragmentation, land management, crop variety, and crop seasonality). For example, $\alpha_{SHO}$ can be altered by the differences in leaf structure/properties (Miller et al. 2016) and leaf wetness (Luyssaert et al. 2014), by the difference in management of both perennial and annual crops and by agricultural practices (Bright et al. 2015; Kaye and Quemada 2017; Robertson et al. 2017).

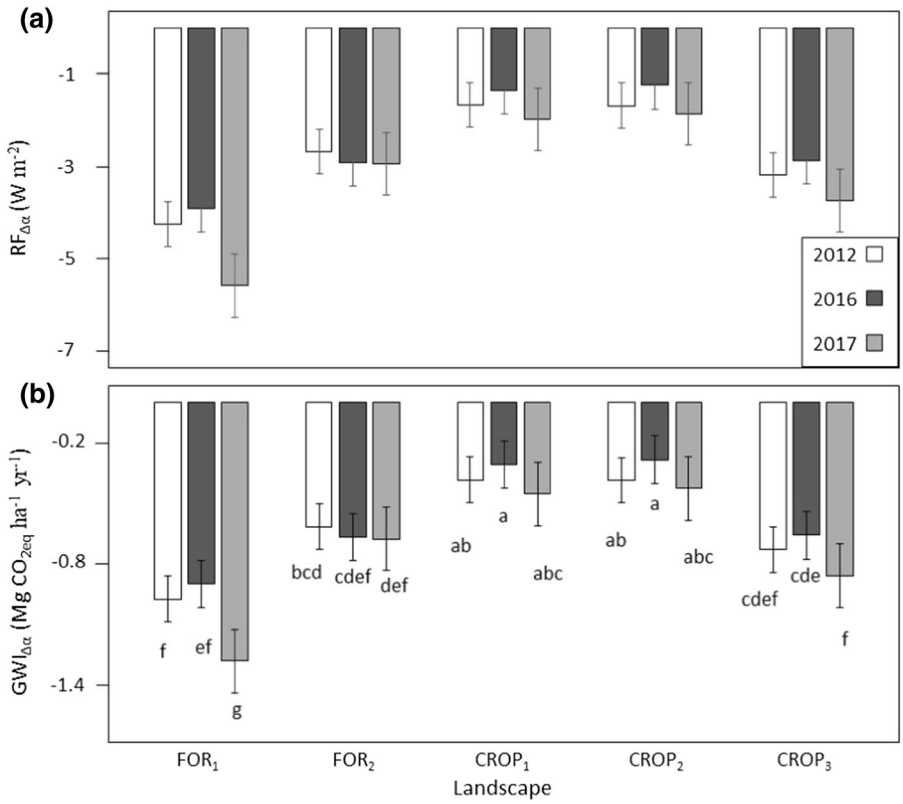


**Fig. 5** Bar chart of $RF_{\Delta\alpha}$ (W m$^{-2}$) due to the difference between mean cropland and mean forest albedos at the top-of-atmosphere across five landscapes at 10:30 a.m. local time (UTC) during the 2012, 2016, and 2017 growing seasons (a). Panel (b) shows $GWI_{\Delta\alpha}$ (Mg $CO_{2eq}$ ha-1 year$^{-1}$) due to the difference between mean cropland and mean forest albedos. Negative values for $RF_{\Delta\alpha}$ and $GWI_{\Delta\alpha}$ indicate cooling effects and $CO_{2eq}$ mitigation impacts, respectively. Bars sharing the same letters are not significantly different (intra- and inter-annual, as well as within and among the five landscapes) according to the Tukey HSD test

The LSM multi-comparison analysis showed that dry conditions led $FOR_1$ to yield statistically higher $\alpha_{SHO}$ compared to wet and normal conditions. On the other hand, $CROP_2$ showed significantly lower $\alpha_{SHO}$ under normal conditions than under dry and wet conditions (Fig. 3a), indicating a different albedo response of forest- and cropland-dominated landscapes to changes in climatic conditions. All other landscapes showed higher $\alpha_{SHO}$ in the dry year (2012) than in the normal and wet years, although not statistically different.

## Albedo-induced radiative forcing (RFΔα) and global warming impact (GWIΔα)

We obtained $RF_{\Delta\alpha}$ (W m$^{-2}$) values that were more representative of the entire growing season through the years 2012, 2016, and 2017. We found that the five landscapes had a negative $RF_{\Delta\alpha}$, indicating a cooling effect. However, such effect was stronger in $FOR_1$ where it ranged between − 3.9 W m$^{-2}$ and − 5.6 W m$^{-2}$ (Table 3; Fig. 5a), followed by $CROP_3$ (− 2.9 W m$^{-2}$ and − 3.7 W m$^{-2}$) and $FOR_2$ (− 2.7 W m$^{-2}$ and − 2.9 W m$^{-2}$), while $CROP_1$ and $CROP_2$ were almost similar (ranging between − 1.2 W m$^{-2}$ and − 1.9 W m$^{-2}$, respectively). In other words, land mosaics in the landscape with the highest proportion of forest (e.g., $FOR_1$) leads to a maximum $RF_{\Delta\alpha}$ of -5.6 W m$^{-2}$ (i.e., a cooling effect), which is similar to that hypothesized by Jiao et al. (2017) under the simulated scenario of global deforestation of evergreen broadleaf forests (local magnitude of $RF_{TOA}$ at − 5.6 W m$^{-2}$). Moreover, in this study we were able to investigate $RF_{\Delta\alpha}$ dynamics across three contrasting precipitation regimes—dry (2012), wet (2016), and normal (2017). The inter-

**Table 3** Mean change of Δα (%), $RF_{\Delta\alpha}$ (W $m^{-2}$), and $GWI_{\Delta\alpha}$ (Mg $CO_{2eq}$ $ha^{-1}$ $year^{-1}$) for each landscape in 2012, 2016, and 2017 growing seasons

| | 2012 | | | 2016 | | | 2017 | | | $diff_{2017–2012}$ | | $diff_{2017–2016}$ | |
|---|---|---|---|---|---|---|---|---|---|---|---|---|---|
| | $\Delta_\alpha$ | $RF_{\Delta\alpha}$ | $GWI_{\Delta\alpha}$ | $\Delta_\alpha$ | $RF_{\Delta\alpha}$ | $GWI_{\Delta\alpha}$ | $\Delta_\alpha$ | $RF_{\Delta\alpha}$ | $GWI_{\Delta\alpha}$ | $\Delta_\alpha$ | $RF_{\Delta\alpha}/GWI_{\Delta\alpha}$ | $\Delta_\alpha$ | $RF_{\Delta\alpha}/GWI_{\Delta\alpha}$ |
| $FOR_1$ | 1.2 (± 0.8) | − 4.2 | − 1.0 | 1.2 (± 0.8) | − 3.9 | − 0.9 | 1.3 (± 0.6) | − 5.6 | − 1.3 | **9.0** | **24.0** | **6.1** | **29.9** |
| $FOR_2$ | 0.8 (± 0.3) | − 2.7 | − 0.6 | 1.0 (± 0.4) | − 2.9 | − 0.7 | 1.1 (± 2.0) | − 2.9 | − 0.7 | 28.5 | 9.0 | 7.8 | 1.4 |
| $CROP_1$ | 0.5 (± 0.2) | − 1.7 | − 0.4 | 0.5 (± 0.3) | − 1.3 | − 0.3 | 0.5 (± 0.3) | − 2.0 | − 0.5 | 9.2 | 15.6 | 12.6 | 32.1 |
| $CROP_2$ | 0.5 (± 0.3) | − 1.7 | − 0.4 | 0.4 (± 0.2) | − 1.2 | − 0.3 | 0.6 (± 1.4) | − 1.9 | − 0.4 | 19.4 | 9.9 | 34.3 | 33.4 |
| $CROP_3$ | 0.9 (± 0.3) | − 3.2 | − 0.7 | 0.9 (± 0.6) | − 2.9 | − 0.7 | 0.9 (± 0.5) | − 3.7 | − 0.9 | 6.0 | 14.9 | **1.0** | **23.3** |

Negative values for $RF_{\Delta\alpha}$ and $GWI_{\Delta\alpha}$ indicate cooling effects and $CO_{2eq}$ mitigation impacts due to albedo change, respectively

Percentage changes (%) between 2017 (baseline) and the two extreme climatic years (i.e., $diff_{2017–2012}$ and $diff_{2017–2016}$, respectively) are also shown. Values with significant decrease (e.g., percent change) are highlighted in bold texts

annual analysis specifically showed that within each landscape, the cooling effect was lower in 2016 and higher in 2017, with the exception of $FOR_2$, which had a lower cooling effect in 2012 and a higher one in 2017 (e.g., slightly higher than in 2016). In sum, accurate quantification of landscape contribution to the global warming potentials needs input from both landscape composition and climate that directly regulate ecosystem properties.

The $GWI_{\Delta\alpha}$ computations enabled us to estimate the $CO_{2eq}$ mitigation caused by the differences between mean cropland and mean forest albedos. Standardized to the same areas, the greatest contribution of albedo change to GWI occurred in the $FOR_1$ ($GWI_{\Delta\alpha}$ = − 1.3 Mg $CO_{2eq}$ $ha^{-1}$ in 2017; Table 3; Fig. 5b), whereas the least contribution occurred in $CROP_2$ (− 0.3 Mg $CO_{2eq}$ $ha^{-1}$ $year^{-1}$). These contributions to GWI are of the same order of magnitude as many crop management components. For example, in this same watershed a corn-soybean-wheat rotation managed with a legume cover crop had a net GWI of 0.4–0.6 Mg $CO_{2eq}$ $ha^{-1}$ $year^{-1}$ (Robertson et al. 2000), without considering albedo change due to historical LULCC. Likewise, the net GWI of conventional and no-till cropping systems were similar in magnitude without consideration of albedo; 0.3 to 0.9 Mg $CO_{2eq}$ $ha^{-1}$ $year^{-1}$, respectively (Gelfand et al. 2013). In several landscapes ($FOR_1$, $FOR_2$, and $CROP_3$), $GWI_{\Delta\alpha}$ was sufficient to offset the GWI costs of both $N_2O$ emissions (0.4 Mg $CO_{2eq}$ $ha^{-1}$ $year^{-1}$) and farming inputs for an alfalfa cropping system (∼ 0.8 Mg $CO_{2eq}$ $ha^{-1}$ $year^{-1}$) (Gelfand et al. 2013).

Surprisingly, the results of inter-annual variation among the three growing seasons showed that the $CO_{2eq}$ mitigation impact between forest- and cropland-dominated ($FOR_1$, $CROP_3$) landscapes was statistically different in 2012 and 2016 for $FOR_1$ (Table 3, Fig. 5a) and in 2016 for $CROP_3$, suggesting that changes in climate conditions, as seen in our study from dry to normal and from wet to normal, can affect the $CO_{2eq}$ mitigation impacts of landscapes. Overall, in one of the forest-dominated landscapes ($FOR_1$) the percent decrease of $CO_{2eq}$ mitigation due to dry and wet conditions was higher than that of the cropland-dominated landscape $CROP_3$ under wet conditions (e.g., lower albedo). Specifically, we found that both dry and wet conditions in $FOR_1$ could significantly reduce $CO_{2\text{-}eq}$. mitigation by up to 24% and ∼ 30% (i.e., percentage change), respectively; while the

$CO_{2eq}$ mitigation's decreasing in $CROP_3$ was significant under wet conditions (e.g., 23.3%), which, in both cases, is still enough to offset 11% of the total $CO_{2eq}$ emissions of conventionally tilled corn systems in the same area and under the same climatic conditions (i.e., 2012 and 2016) (Abraha et al. 2019). Surprisingly the high decrease in $\Delta\alpha$ (e.g., $FOR_1$: 9% vs 6.1% and $CROP_3$: 6% vs 1%) under wet conditions did not lead to a high decrease in $CO_{2eq}$ mitigation.

## Assumptions, limitations and uncertainties

The methodology used in this study represents an analytical approach as a proof of concept of the effects of landscape patches and climatic conditions on $RF_{\Delta\alpha}$ and $GWI_{\Delta\alpha}$ in the context of forest- and cropland-dominant landscapes. However, certain assumptions can be made on the application of our approach. The first is that $RF_{\Delta\alpha}$ is related to land mosaics (e.g., patch composition) derived by land transformation (Muñoz et al. 2010). In fact, the focus of the present study is to measure the changes in $RF_{\Delta\alpha}$ and $GWI_{\Delta\alpha}$ due to conversion of forests to croplands, assuming the existing croplands were forests in the past. We then considered $\Delta\alpha$ using the baseline (forest), which is treated as a reference cover type of the five landscapes, since it was the dominant land cover type of the pre-European settlements (Brown et al. 2000).

A second assumption is related to using in situ incoming radiation ($SW_{in}$) for the calculation of upward atmospheric transmittance ($T_a$). While the literature (Lenton and Vaughan 2009; Muñoz et al. 2010; Cherubini et al. 2012) refers to $T_a$ as the annual global mean ($T_a = 0.854$) for a constant zenith angle of 60°, here we calculated $T_a$ for a given day as the ratio $SW_{in}/SW_{TOA}$, with $SW_{in}$ obtained from in situ measurements within the study area (Abraha et al. 2015), specifically at the $FOR_2$ landscape. By avoiding such a default value for $T_a$ (e.g., 0.845), we reduced the error by $\sim$ 30%. We then assumed that $SW_{in}$ would be the same at all five landscape locations. In fact, unlike previous studies, we calculated $RF_{\Delta\alpha}$ and $GWI_{\Delta\alpha}$ on a relatively small area (i.e., not global/regional) for which the uncertainty error carried by a constant $T_a$ would not have been significant.

A third assumption is related to the time horizon (TH) fixed at 100 years, which is the same time horizon used in the Kyoto Protocol (Boucher et al. 2009). By calculating the annual $GWI_{\Delta\alpha}$ as 1/100 of the total $CO_{2eq}$, we assumed that, in each landscape, the same land mosaic will be maintained for the duration of 100 years. This choice of TH is a limitation because short time horizons can overemphasize the impacts of albedo, while long time horizons can de-emphasize the impacts (Anderson-Teixeira et al. 2012).

Another limitation of the study is the use of a growing season (March–October) time frame for $RF_{\Delta\alpha}$ and $GWI_{\Delta\alpha}$ rather than an annual period. Previous studies (Campbell and Norman 1998; Bonan 2008; Iqbal 2012; Liang et al. 2013; Zhao and Jackson 2014; Bright et al. 2015; Kaye and Quemada 2017; Sun et al. 2017) have addressed the importance of snow cover to variability/uncertainty of albedo between forest and cropland because of the capability of forest stands of masking the snow (e.g., lowing the albedo). Nevertheless, our use of growing season values allowed to better isolate the human disturbance on the landscape through agricultural activities by focusing on the crop phenology and its relation with climatic conditions. Had we included wintertime albedo, our forest-cropland differences would have been even greater, however, since deciduous forest stands have higher wintertime albedo than cropland due to the presence of bare branches (Bonan 2008; Anderson et al. 2011) during winter. On the other hand, from the remote sensing perspective, MODIS snow-albedo retrievals have been demonstrated to be less accurate than acquisitions during the growing season (Wang et al. 2014).

There are also uncertainties associated with user-defined data (Muñoz et al. 2010), such as considering $\Delta\alpha$ as the difference between croplands and forest albedos. AF (i.e., $CO_2$ airborne fraction) and $rf_{CO_2}$ (the marginal RF of $CO_2$ emissions at the current atmospheric concentration) are estimated to embed errors of $\pm$ 15% and $\pm$ 10%, respectively, in the GWI estimation (Forster et al. 2007; Akbari et al. 2009). It is also worth mentioning the uncertainties related to the scale-dependency. In fact, there is a mismatch between the spatial representativeness of MODIS acquisition pixels (e.g., 500 $\times$ 500 m) and that of Landsat (30 $\times$ 30 m), which leads to intrinsic variability of the measurements (Chrysoulakis et al. 2018; Chen et al. 2019). However, as already emphasized in previous studies (Mira et al. 2015; Moustafa et al. 2017), validation techniques provide a reasonable estimate of albedo from MODIS products across

homogeneous landscapes (e.g., the two forest- and the three cropland-dominated landscapes).

Lastly, we did not consider the effect of spatial autocorrelation that may affect the significance of the statistic test (Fletcher and Fortin 2018). Nevertheless, the aim of this study is not to attempt spatial predictions (Feilhauer et al. 2012) of $RF_{\Delta\alpha}$ and $GWI_{\Delta\alpha}$.

## Conclusions

1. There are significant contributions ($R^2 = 0.64$) to the overall variation in albedo due to landscapes (i.e., ecoregions), cover types (i.e., landscape mosaics), and seasons (i.e., seasonality). Variation in seasons contributes more than landscape composition ($\sim$ 16% and 11%, respectively) in variations of albedo.
2. By integrating spatial (e.g., five landscapes within ecoregions) and temporal (e.g., inter- and intra-annual) patterns as main drivers of albedo variation, we found that cropland-dominated landscapes produce a higher intra-annual variability of albedo under dry, wet, and normal climatic conditions, likely due to more frequent disturbances (i.e., management activities). Forest-dominated landscapes have higher albedo in dry and wet years than that in normal years, whereas only one crop-dominated landscape shows statistically lower albedo under normal conditions than that under dry and wet ones. This indicates a different response to changes in climatic conditions from forest- and cropland-dominated landscapes.
3. The cooling effect of $RF_{\Delta\alpha}$ occurs in all landscapes but is higher in the landscape with the highest proportion of forests ($FOR_1$) (e.g., higher differences between mean cropland and mean forest albedos). The pattern of $GWI_{\Delta\alpha}$ across the five landscapes is similar to that of $RF_{\Delta\alpha}$, with $CO_{2eq}$ mitigation relative to pre-existing forest vegetation higher in $FOR_1$ and lower in $CROP_1$ and $CROP_2$.
4. We found that in the landscape with the highest proportion of forest ($FOR_1$) both dry and wet conditions can significantly reduce $CO_{2eq}$ mitigation by up to 24% and $\sim$ 30%, respectively; while the reduction of $CO_{2eq}$ mitigation is significant only in one of the cropland-dominated landscapes ($CROP_3$) under wet conditions (e.g., 23.3% decrease).

**Acknowledgements** This study was supported, in part, by the NASA Carbon Cycle & Ecosystems program (NNX17AE16G), the Great Lakes Bioenergy Research Center funded by the U.S. Department of Energy, Office of Science, Office of Biological and Environmental Research under Award Numbers DE-SC0018409 and DE-FC02-07ER64494 and the Natural Science Foundation Long-term Ecological Research Program (DEB 1637653) at the Kellogg Biological Station, the NASA Science of Terra and Aqua program (NNX14AJ32G). We wish to thank Dr. Geoffrey Henebry for helpful suggestions and comments during the post-review process. We also thank the two anonymous reviewers who helped improving the quality of our manuscript.

## References

Abraha M, Chen J, Chu H, Zenone T, John R, Su YJ, Hamilton SK (2015) Evapotranspiration of annual and perennial biofuel crops in a variable climate. Glob Change Biol Bioenergy 7:1344–1356

Abraha M, Gelfand I, Hamilton SK, Shao C, Su YJ, Robertson JP, Chen J (2016) Ecosystem water-use efficiency of annual corn and perennial grasslands: contributions from land-use history and species composition. Ecosystems 19:1001–1012

Abraha M, Gelfand I, Hamilton SK, Shao C, Su YJ, Chen J, Robertson JP (2019) Carbon debt of field-scale conservation reserve program grasslands converted to annual and perennial bioenergy crops. Environ Res Lett 14:024019. https://doi.org/10.1088/1748-9326/aafc10

Akbari H, Menon S, Rosenfeld A (2009) Global cooling: increasing world-wide urban albedos to offset $CO_2$. Clim Change 94:275–286

Anderson RG, Canadell JG, Randerson JT, Jackson RB, Hungate BA, Baldocchi DD, Ban-Weiss GA, Bonan GB, Caldeira K, Cao L, Diffenbaugh NS, Gurney KR, Kueppers LM, Law BE, Luyssaert S, O'Halloran TL (2011) Biophysical considerations in forestry for climate protection. Front Ecol Environ 9:174–182. https://doi.org/10.1890/090179

Anderson-Teixeira KJ, Snyder PK, Twine TE, Cuadra SV, Costa MH, DeLucia EH (2012) Climate-regulation services of natural and agricultural ecoregions of the Americas. Nat Clim Change 2:177–181

Antón A, Cebrian J, Heck KL, Duarte CM, Sheehan KL, Miller M-EC, Foster CD (2011) Decoupled effects (positive to negative) of nutrient enrichment on ecosystem services. Ecol Appl 21:991–1009. https://doi.org/10.1890/09-0841.1

Bala G, Caldeira K, Wickett M, Phillips TJ, Lobell DB, Delire C, Mirin A (2007) Combined climate and carbon-cycle effects of large-scale deforestation. Proc Natl Acad Sci USA 104:6550–6555

Barnes CA, Roy DP (2010) Radiative forcing over the conterminous United States due to contemporary land cover land use change and sensitivity to snow and interannual albedo variability. J Geophys Res Biogeosciences 115:G04033. https://doi.org/10.1029/2010JG001428

Bennett AF, Radford JQ, Haslem A (2006) Properties of land mosaics: implications for nature conservation in agricultural environments. Biol Conserv 133:250–264

Berbet MLC, Costa MH (2003) Climate change after tropical deforestation: seasonal variability of surface albedo and its effects on precipitation change. J Clim 16:2099–2104. https://doi.org/10.1175/1520-0442(2003)016%3c2099:CCATDS%3e2.0.CO;2

Betts RA (2000) Offset of the potential carbon sink from boreal forestation by decreases in surface albedo. Nature 408:187–190

Betts RA (2001) Biogeophysical impacts of land use on present-day climate: near-surface temperature change and radiative forcing. Atmos Sci Lett 2:39–51. https://doi.org/10.1006/asle.2001.0037

Bird DN, Kunda M, Mayer A, Schlamadinger B, Canella L, Johnston M (2008) Incorporating changes in albedo in estimating the climate mitigation benefits of land use change projects. Biogeosci Discuss 5:1511–1543

Bonan GB (2008) Forests and climate change: forcings, feedbacks, and the climate benefits of forests. Science 320:1444–1449

Bonan GB (2016) Ecological climatology: concepts and applications. Cambridge University Press, Cambridge, p 723

Boucher O, Friedlingstein P, Collins B, Shine KP (2009) The indirect global warming potential and global temperature change potential due to methane oxidation. Environ Res Lett 4:044007

Bright RM (2015) Metrics for biogeophysical climate forcings from land use and land cover changes and their inclusion in life cycle assessment: a critical review. Environ Sci Technol 49:3291–3303

Bright RM, Zhao K, Jackson RB, Cherubini F (2015) Quantifying surface albedo and other direct biogeophysical climate forcings of forestry activities. Glob Change Biol 21:3246–3266

Brovkin V, Boysen L, Raddatz T, Gayler V, Loew A, Claussen M (2013) Evaluation of vegetation cover and land-surface albedo in MPI-ESM CMIP5 simulations. J Adv Model Earth SY 5:48–57

Brown DG, Pijanowski BC, Duh JD (2000) Modeling the relationships between land use and land cover on private lands in the Upper Midwest, USA. J Environ Manage 59:247–263

Burton VB, Zak DR, Denton SR, Spurr SH (1998) Forest ecology. 4th Edition. pp 225-240, New York

Cai H, Wang J, Wang Y, Wang M, Qin Z, Dunn B (2016) Consideration of land use change-induced surface albedo effects in life-cycle analysis of biofuels. Energy Environ Sci 9:2855–2867

Campbell GS, Norman JM (1998) Introduction to environmental biophysics, 2nd edn. Springer, New York, p 286

Carrer D, Pique G, Ferlicoq M, Ceamanos X, Ceschia E (2018) What is the potential of cropland albedo management in the fight against global warming? A case study based on the use of cover crops. Environ Res Lett 13:044030

Chen J, Brosofske KD, Noormets A, Crow TR, Bresee MK, Le Moine JM, Euskirchen ES, Mather SV, Zheng D (2004) A working framework for quantifying carbon sequestration in disturbed land mosaics. Environ Manage 33:S210–S221

Chen J, Sciusco P, Ouyang Z, Zhang R, Henebry GM, John R, Roy DP (2019) Linear downscaling from MODIS to Landsat: connecting landscape composition with ecosystem functions. Landsc Ecol 34:2917–2934

Chen J, Wan S, Henebry GM, Qi J, Gutman G, Sun G, Kappas M (2013) Dryland East Asia: land dynamics amid social and climate change. Walter de Gruyter, Berlin, Boston, p 470

Cherubini F, Bright RM, Strømman AH (2012) Site-specific global warming potentials of biogenic $CO_2$ for bioenergy: contributions from carbon fluxes and albedo dynamics. Environ Res Lett 7:045902

Chrysoulakis N, Mitraka Z, Gorelick N (2018) Exploiting satellite observations for global surface albedo trends monitoring. Theor Appl Climatol 137:1171–1179

Culf AD, Fisch G, Hodnett MG (1995) The albedo of Amazonian forest and ranch land. J Clim 8:1544–1554

Davin EL, de Noblet-Ducoudré N, Friedlingstein P (2007) Impact of land cover change on surface climate: relevance of the radiative forcing concept. Geophys Res Lett 34:L13702

Davin EL, Seneviratne SI, Ciais P, Olioso A, Wang T (2014) Preferential cooling of hot extremes from cropland albedo management. Proc Natl Acad Sci USA 111:9757–9761

Dickinson RE (1983) Land surface processes and climate—surface albedos and energy balance. Adv Geophys 25:305–353

Eagle AJ, Henry LR, Olander LP, Haugen-Kozyra K, Millar N, Robertson GP (2010) Greenhouse gas mitigation potential of agricultural land management in the United States. A Synthesis of the Literature. Technical Working Group on Agricultural Greenhouse Gases (T-AGG) Report 68p

Eagle AJ, Henry LR, Olander LP, Haugen-Kozyra K, Millar N, Robertson GP (2012) Greenhouse gas mitigation potential of agricultural land managementin the United States: A synthesis of the literature. Report NIR, 10-04, 72p.

Euskirchen ES, Chen J, Li H, Gustafson EJ, Crow TR (2002) Modeling landscape net ecosystem productivity (LandNEP) under alternative management regimes. Ecol Model 154:75–91

Feilhauer H, He KS, Rocchini D (2012) Modeling species distribution using niche-based proxies derived from composite bioclimatic variables and MODIS NDVI. Remote Sens 4:2057–2075

Fletcher R, Fortin M-J (2018) Spatial dependence and autocorrelation. In: Fletcher R, Fortin M-J (eds) Spatial ecology and conservation modeling: applications with R. Springer International Publishing, Cham, pp 133–168

Forster P, Ramaswamy V, Artaxo P, Berntsen T, Betts R, Fahey DW, Haywood J, Lean J, Lowe DC, Raga G, Schulz M, Dorland RV, Bodeker G, Etheridge D, Foukal P, Geller FM, Joos F, Keeling CD, Keeling R, Kinne S, Lassey K, Oram D, O'Shaughnessy K, Ramankutty N, Reid G, Rind D, Rosenlof R, Sausen R, Schwarzkopf D, Solanki SK, Stenchikov G, Stuber N, Takemura T, Textor C, Wang R, Weiss R, Whorf T, Nakajima T, Ramanathan V, Ramaswamy V, Artaxo P, Berntsen T, Betts R, Fahey DW, Haywood J, Lean J, Lowe DC, Myhre G, Nganga J, Prinn

R, Raga G, Schulz M, Dorland RV (2007) Changes in atmospheric constituents and in radiative forcing. J Clim 25:527–542

Fuglestvedt JS, Berntsen TK, Godal O, Sausen R, Shine KP, Skodvin T (2003) Metrics of climate change: assessing radiative forcing and emission indices. Clim Change 58:267–331

Gelfand I, Robertson GP (2015) Mitigation of greenhouse gas emissions in agricultural ecosystems. In: Hamilton SK, Doll JE, Robertson GP (eds) The ecology of agricultural landscapes: long-term research on the path to sustainability. Oxford University Press, New York, pp 310–339

Gelfand I, Sahajpal R, Zhang X, Izaurralde RC, Gross KL, Robertson GP (2013) Sustainable bioenergy production from marginal lands in the US Midwest. Nature 493:514–517

Georgescu M, Lobell DB, Field CB (2011) Direct climate effects of perennial bioenergy crops in the United States. Proc Natl Acad Sci USA 108:4307–4312

Goosse H (2015) Climate system dynamics and modeling. Cambridge University Press, Cambridge, p 357

Gorelick N, Hancher M, Dixon M, Ilyushchenko S, Thau D, Moore R (2017) Google Earth Engine: planetary-scale geospatial analysis for everyone. Remote Sens Environ 202:18–27

Govindasamy B, Duffy PB, Caldeira K (2001) Land use changes and northern hemisphere cooling. Geophys Res Lett 28:291–294

Gray V (2007) Climate Change 2007: the physical science basis summary for policymakers. Energy Environ 18:433–440

Haas G, Wetterich F, Köpke U (2001) Comparing intensive, extensified and organic grassland farming in southern Germany by process life cycle assessment. Agric Ecosyst Environ 83:43–53

Haines A (2003) Climate change 2001: the scientific basis. Contribution of working group 1 to the third assessment report of the intergovernmental panel on climate change. Houghton JT, Ding Y, Griggs DJ, Noguer M, van Der Winden PJ, Dai X. Cambridge: Cambridge University Press, 2001, Pp.881, £34.95 (HB) ISBN: 0-21-01495-6; £90.00 (HB) ISBN: 0-521-80767-0. Int J Epidemiol 32(2):321

Haralick RM, Shanmugam K, Dinstein I (1973) Textural features for image classification. IEEE Trans Syst Man Cybern SMC 3:610–621

Henderson-Sellers A, Wilson MF (1983) Surface albedo data for climatic modeling. Rev Geophys 21:1743–1778

Houspanossian J, Giménez R, Jobbágy E, Nosetto M (2017) Surface albedo raise in the South American Chaco: combined effects of deforestation and agricultural changes. Agric For Meteorol 232:118–127

Iqbal M (2012) An Introduction to Solar Radiation. Elsevier, New York, 390p

Jeong SJ, Ho C-H, Gim HJ, Brown ME (2011) Phenology shifts at start vs. end of growing season in temperate vegetation over the Northern Hemisphere for the period 1982–2008. Glob Change Bio 17:2385–2399

Jeong SJ, Ho CH, Piao S, Kim J, Ciais P, Lee YB, Jhun JG, Park SK (2014) Effects of double cropping on summer climate of the North China Plain and neighbouring regions. Nat Clim Change 4:615–619

Jiao T, Williams A, Ghimire B, Masek J, Gao F, Schaaf C (2017) Global climate forcing from albedo change caused by large-scale deforestation and reforestation: quantification and attribution of geographic variation. Clim Change 142:463–476

Kaye JP, Quemada M (2017) Using cover crops to mitigate and adapt to climate change. A review. Agron Sustain Dev 37:4

Lee X, Goulden ML, Hollinger DY, Barr A, Black TA, Bohrer G, Bracho R, Drake B, Goldstein A, Gu L, Katul G, Kolb T, Law BE, Margolis H, Meyers T, Monson R, Munger W, Oren R, Paw UKT, Richardson AD, Schmid HP, Staebler R, Wofsy S, Zhao L (2011) Observed increase in local cooling effect of deforestation at higher latitudes. Nature 479:384–387

Lenton TM, Vaughan NE (2009) The radiative forcing potential of different climate geoengineering options. Atmos Chem Phys 9:5539–5561

Li B, Gasser T, Ciais P, Piao S, Tao S, Balkanski Y, Hauglustaine D, Boisier JP, Chen Z, Huang M, Li LZ, Li Y, Liu H, Liu J, Peng S, Shen Z, Sun Z, Wang R, Wang T, Yin G, Yin Y, Zeng Z, Zhou F (2016) The contribution of China's emissions to global climate forcing. Nature 531(7594):357

Li J, Wang XR, Wang XJ, Ma WC, Zhang H (2009) Remote sensing evaluation of urban heat island and its spatial pattern of the Shanghai metropolitan area, China. Ecol Complex 6:413–420

Liang S, Zhao X, Liu S, Yuan W, Cheng X, Xiao Z, Zhang X, Liu Q, Cheng J, Tang H, Qu Y, Bo Y, Qu Y, Ren H, Yu K, Townshend J (2013) A long-term Global LAnd Surface Satellite (GLASS) data-set for environmental studies. Int J Digit Earth 6:5–33

Loarie SR, Lobell DB, Asner GP, Mu Q, Field CB (2011) Direct impacts on local climate of sugar-cane expansion in Brazil. Nat Clim Change 1:105–109

Luyssaert S, Jammet M, Stoy PC, Estel S, Pongratz J, Ceschia E, Churkina G, Don A, Erb K, Ferlicoq M, Gielen B, Grünwald T, Houghton RA, Klumpp K, Knohl A, Kolb T, Kuemmerle T, Laurila T, Lohila A, Loustau D, McGrath MJ, Meyfroidt P, Moors EJ, Naudts K, Novick K, Otto J, Pilegaard K, Pio CA, Rambal S, Rebmann C, Ryder J, Suyker AE, Varlagin A, Wattenbach Dolman AJ (2014) Land management and land-cover change have impacts of similar magnitude on surface temperature. Nat Clim Change 4:389–393

Mallya G, Zhao L, Song XC, Niyogi D, Govindaraju RS (2013) 2012 Midwest drought in the United States. J Hydrol Eng 18:737–745

Matthews HD, Weaver AJ, Eby M, Meissner KJ (2003) Radiative forcing of climate by historical land cover change. Geophysical Res Lett. https://doi.org/10.1525/bio.2013.63.4.6

Merlin O (2013) An original interpretation of the wet edge of the surface temperature-albedo space to estimate crop evapotranspiration (SEB-1S), and its validation over an irrigated area in northwestern Mexico. Hydrol Earth Sysy Sci 17:3623–3637

Michigan State Climatologist's Office (2013). Gull Lake (3504). Michigan State University. Retrieved from http://climate.geo.msu.edu/climate_mi/stations/3504/

Miller JN, VanLoocke A, Gomez-Casanovas N, Bernacchi CJ (2016) Candidate perennial bioenergy grasses have a

higher albedo than annual row crops. Glob Change Biol Bioenergy 8:818–825
Mira M, Weiss M, Baret F, Courault D, Hagolle O, Gallego-Elvira B, Olioso A (2015) The MODIS (collection V006) BRDF/albedo product MCD43D: temporal course evaluated over agricultural landscape. Remote Sens Environ 170:216–228
Moustafa SE, Rennermalm AK, Román MO, Wang Z, Schaaf CB, Smith LC, Koenig LS, Erb A (2017) Evaluation of satellite remote sensing albedo retrievals over the ablation area of the southwestern Greenland ice sheet. Remote Sens Environ 198:115–125
Muñoz I, Campra P, Fernández-Alba AR (2010) Including $CO_2$-emission equivalence of changes in land surface albedo in life cycle assessment. Methodology and case study on greenhouse agriculture. Int J Life Cycle Assess 15:672–681
Omernik JM, Griffith GE (2014) Ecoregions of the conterminous United States: evolution of a hierarchical spatial framework. Environ Manage 54:1249–1266
Peters GP, Aamaas B, Lund MT, Solli C, Fuglestvedt JS (2011) Alternative "global warming" metrics in life cycle assessment: a case study with existing transportation data. Environ Sci Technol 45:8633–8641
Picard G, Domine F, Krinner G, Arnaud L, Lefebvre E (2012) Inhibition of the positive snow-albedo feedback by precipitation in interior Antarctica. Nat Clim Change 2:795–798
Pielke RA, Pitman A, Niyogi D, Mahmood R, McAlpine C, Hossain F, Goldewijk KK, Nair U, Betts R, Fall S, Reichstein M, Kabat P, deNoblet N (2011) Land use/land cover changes and climate: modeling analysis and observational evidence. Wiley Interdiscip Rev Clim Change 2:828–850
Poeplau C, Don A (2015) Carbon sequestration in agricultural soils via cultivation of cover crops – a meta-analysis. Agric Ecosyst Environ 200:33–41
Raudsepp-Hearne C, Peterson GD, Tengö M, Bennett EM, Holland T, Benessaiah K, MacDonald GK, Pfeifer L (2010) Untangling the environmentalist's paradox: why is human well-being increasing as ecosystem services degrade? Bioscience 60:576–589
Robertson GP, Hamilton SK, Barham BL, Dale BE, Izaurralde RC, Jackson RD, Landis DA, Swinton SM, Thelen KD, Tiedje JM (2017) Cellulosic biofuel contributions to a sustainable energy future: choices and outcomes. Science 356:1349
Robertson GP, Paul EA, Harwood RR (2000) Greenhouse gases in intensive agriculture: contributions of individual gases to the radiative forcing of the atmosphere. Science 289:1922–1925
Román MO, Schaaf CB, Woodcock CE, Strahler AH, Yang X, Braswell RH, Curtis PS, Davis KJ, Dragoni D, Goulden ML (2009) The MODIS (collection V005) BRDF/albedo product: assessment of spatial representativeness over forested landscapes. Remote Sens Environ 113:2476–2498
Schaetzl RJ, Darden JT, Brandt DS (2009) Michigan geography and geology. Pearson Learning Solutions
Seidl R, Spies TA, Peterson DL, Stephens SL, Hicke JA (2016) Searching for resilience: addressing the impacts of changing disturbance regimes on forest ecosystem services. J Appl Ecol 53:120–129
Shao C, Li L, Dong G, Chen J (2014) Spatial variation of net radiation and its contribution to energy balance closures in grassland ecosystems. Ecol Process 3:7
Smith P, Martino D, Cai Z, Gwary D, Janzen H, Kumar P, McCarl B, Ogle S, O'Mara F, Rice C, Scholes B, Sirotenko O, Howden M, McAllister T, Pan G, Romanenkov V, Schneider U, Towprayoon S, Wattenbach M, Smith J (2008) Greenhouse gas mitigation in agriculture. Philos Trans R So B: Biol Sci 363:789–813
Storelvmo T, Leirvik T, Lohmann U, Phillips PC, Wild M (2016) Disentangling greenhouse warming and aerosol cooling to reveal Earth's climate sensitivity. Nat Geosci 9:286
Sun Q, Wang Z, Li Z, Erb A, Schaaf CB (2017) Evaluation of the global MODIS 30 arc-second spatially and temporally complete snow-free land surface albedo and reflectance anisotropy dataset. Int J Appl Earth Obs Geoinformation 58:36–49
Team RC (2017) R: A language and environment for statistical computing. R Foundation for Statistical Computing, Vienna, Austria. https://www.Rproject.org
Tian L, Chen J, Shao C (2018) Interdependent dynamics of LAI-albedo across the roofing landscapes: Mongolian and Tibetan Plateaus. Remote Sens 10:1159
Wang D, Liang S, He T, Yu Y, Schaaf C, Wang Z (2015) Estimating daily mean land surface albedo from MODIS data. J Geophys Res Atmos 120:4825–4841
Wang K, Liu J, Zhou X, Sparrow M, Ma M, Sun Z, Jiang W (2004) Validation of the MODIS global land surface albedo product using ground measurements in a semidesert region on the Tibetan Plateau. J Geophys Res Atmos 109:D05107
Wang Z, Crystal BS, Alan HS, Mark JC, Miguel OR, Yanmin S, Curtis EW, David YH, David RF (2014) Evaluation of MODIS Albedo Product (MCD43A) over grassland, agriculture and forest surface types during dormant and snow-covered periods. Remote Sens Environ 140:60–77
Yuan ZY, Chen HYH (2015) Decoupling of nitrogen and phosphorus in terrestrial plants associated with global changes. Nat Clim Change 5:465–469
Zhang Y, Wang X, Pan Y, Hu R (2013) Diurnal and seasonal variations of surface albedo in a spring wheat field of arid lands of Northwestern China. Int J Biometeorol 57:67–73
Zhao K, Jackson RB (2014) Biophysical forcings of land-use changes from potential forestry activities in North America. Ecol Monogr 84:329–353
Zheng L, Zhao G, Dong J, Ge Q, Tao J, Zhang X, Qi Y, Doughty RB, Xiao X (2019) Spatial, temporal, and spectral variations in albedo due to vegetation changes in China's grasslands. ISPRS J Photogramm Remote Sens 152:1–12

Supplementary materials for:

# Spatiotemporal variations of albedo in managed agricultural landscapes: Inferences to global warming impacts (GWI)

Pietro Sciusco[1,2*], Jiquan Chen[1,2], Michael Abraha[2,3,4], Cheyenne Lei[1,2], G. Philip Robertson[3,4], Raffaele Lafortezza[5,6,2], Gabriela Shirkey[1,2], Zutao Ouyang[7], Rong Zhang[8,9], Ranjeet John[10]

[1] Department of Geography, Environment & Spatial Sciences, Michigan State University, East Lansing, MI, 48823, USA

[2] Center for Global Change and Earth Observations, Michigan State University, East Lansing, MI, 48823, USA

[3] Great Lakes Bioenergy Research Center, Michigan State University, East Lansing, MI, 48824, USA

[4] W.K. Kellogg Biological Station, Michigan State University, Hickory Corners, MI, 49060, USA

[5] Department of Agricultural and Environmental Sciences, University of Bari "A. Moro", Bari, 70126, Italy

[6] Department of Geography, The University of Hong Kong, Centennial Campus, Pokfulam Road, Hong Kong

[7] Department of Earth System Science, Stanford University, Stanford, CA, 94305, USA

[8] Zhejiang Tiantong Forest Ecosystem National Observation and Research Station, School of Ecological and Environmental Sciences, East China Normal University, Shanghai, 200241, China

[9] Center for Global Change and Ecological Forecasting, East China Normal University, Shanghai, 200062, China

[10] Department of Biology, University of South Dakota, Vermillion, SD, 57069, USA

* Corresponding author: Pietro Sciusco; Email: sciuscop@msu.edu; Phone: 517-505-1074

Date of manuscript revision: 02/19/2020

This file contains:

Tables S1 and S2

**Table S1** Description of the five Level IV ecoregions that fall within the Kalamazoo River watershed boundary. Additional information can be found online at EPA: https://www.epa.gov/eco-research/ecoregion-download-files-state-region-5#pane-20

| Level IV ecoregions | | |
|---|---|---|
| Full name | Abbreviation | Features |
| Battle Creek Outwash Plain | 56b | **Landforms**: broad, flat plain, major drainage during the Pleistocene glaciers receding.<br>**Soils**: well-drained loamy soils (pasture) and sandy soils suitable for corn, soybeans, and grain.<br>**Pre-settlement vegetation**: wet and dry tallgrass prairies, oak savanna. |
| Michigan Lake Plain | 56d | **Landforms**: sandy coastal strip with beaches, high dunes, beaches ridges, mucky inter-dune depressions, and swales.<br>**Soils**: excessively-drained (oak and white pine), poorly-drained (marsh grasses, aspen, silver maple), and well-drained sandy soils (pasture, hay, aspen, cherry, oak, white pine).<br>**Pre-settlement vegetation**: pine, hemlock, beech, sugar maple, treeless marshes, lowland hardwood swamps, and tamarack swamp. |
| Lake Michigan Moraines | 56f | **Landforms**: end and ground moraine.<br>**Soils**: well-drained sandy loams soils (row crops, orchards, oak-hickory-sugar maple forests), poorly-drained sandy and clay loams soils (marsh grasses, aspen, silver maple), finer-textured, less permeable soils (beech-sugar maple forests).<br>**Pre-settlement vegetation**: beech, sugar maple, oak, oak savanna, oak-hickory, hemlock. |
| Lansing Loamy Plain | 56g | **Landforms**: ground moraine, well-drained hills, and poorly-drained linear depressions.<br>**Soils**: medium-textured loamy soils (beech-sugar maple forests), sandy soils (pasture or hay), poorly-drained soils (marsh grasses, aspen, silver maple, and swamp white oak).<br>**Pre-settlement vegetation**: beech-sugar maple forests, associated with basswood, black maple, red oak, and white maple forests (ground moraines), oak-hickory forests (drier end moraines), American elm, red ash, silver maple, tamarack, swamp white oak, and wet prairies (poorly drained linear depressions). |
| Interlobate Dead Ice Moraines | 56h | **Landforms**: coarse-textured end moraine, kames, and outwash sands.<br>**Soils**: sandy loams soils (corn, soybeans, and grain), poorly-drained sandy loams soils (marsh grasses, aspen, and silver maple), well-drained soils (pasture and oak-hickory forests).<br>**Pre-settlement vegetation**: oak savanna, oak-hickory forests, wet and dry tallgrass prairies. |

**Table S2** Mean (±sd) of $\alpha_{SHO}$ (%) by cover type and landscapes during the 2012 (dry), 2016 (wet) and 2017 (normal). Mean values ($\overline{X}$; %) represent the three years.

| | | Cover type | | | | | | | |
|---|---|---|---|---|---|---|---|---|---|
| Landscape | | Urban | Cropland | Barrens | Forest | Water | Wetlands | Grasslands | All |
| $FOR_1$ | 2012 | 15.1 (±0.7) | 16.0 (±0.7) | 14.6 (±0.5) | 14.6 (±0.6) | 13.8 (±0.6) | 14.2 (±0.8) | 15.4 (±0) | 14.7 (±0.8) |
| | 2016 | 14.7 (±0.7) | 15.8 (±0.9) | 14.2 (±0.6) | 14.3 (±0.6) | 13.7 (±0.4) | 14.1 (±0.8) | 14.9 (±0) | 14.4 (±0.9) |
| | 2017 | 14.7 (±0.8) | 15.9 (±1.0) | 14.0 (±0.7) | 14.1 (±0.7) | 13.6 (±0.5) | 14.0 (±0.8) | 15.0 (±0) | 14.3 (±1.0) |
| | $\overline{X}$ | 14.8 | 15.9 | 14.2 | 14.3 | 13.7 | 14.1 | 15.1 | 14.6 |
| $FOR_2$ | 2012 | 14.1 (±1.8) | 15.2 (±1.0) | 14.8 (±0.6) | 14.4 (±1.2) | 9.3 (±3.5) | 14.4 (±1.1) | 14.3 (±1.3) | 14.1 (±2.3) |
| | 2016 | 14.0 (±1.9) | 15.3 (±1.2) | 14.8 (±0.7) | 14.2 (±1.5) | 9.1 (±3.6) | 14.3 (±1.2) | 13.9 (±1.5) | 14.0 (±2.4) |
| | 2017 | 13.6 (±1.9) | 14.8 (±1.1) | 14.3 (±0.7) | 13.7 (±1.3) | 8.7 (±3.5) | 8.7 (±1.2) | 13.5 (±1.7) | 13.5 (±2.3) |
| | $\overline{X}$ | 13.9 | 15.1 | 14.6 | 14.1 | 9.0 | 14.2 | 13.9 | 13.9 |
| $CROP_1$ | 2012 | 16.8 (±0.5) | 16.9 (±0.7) | 16.5 (±0) | 16.4 (±0.9) | 16.5 (±0.1) | 16.4 (±0.7) | 16.3 (±1.0) | 16.8 (±0.7) |
| | 2016 | 17.1 (±0.6) | 17.1 (±0.8) | 16.5 (±0) | 16.6 (±1.0) | 16.2 (±0.4) | 16.6 (±0.8) | 16.1 (±1.2) | 17.0 (±0.8) |
| | 2017 | 16.9 (±0.6) | 17.0 (±0.7) | 16.5 (±0) | 16.5 (±0.9) | 16.2 (±0.2) | 16.4 (±0.8) | 16.0 (±1.7) | 16.8 (±0.8) |
| | $\overline{X}$ | 16.9 | 17.0 | 16.5 | 16.5 | 16.3 | 16.5 | 16.1 | 16.7 |
| $CROP_2$ | 2012 | 16.0 (±1.0) | 16.7 (±0.5) | 16.0 (±0) | 16.3 (±0.5) | 15.3 (±0.8) | 16.1 (±0.5) | 16.0 (±0) | 16.5 (±0.6) |
| | 2016 | 16.0 (±1.0) | 16.7 (±0.5) | 16.3 (±0) | 16.3 (±0.6) | 15.6 (±0.6) | 16.1 (±0.5) | 15.9 (±0) | 16.5 (±0.6) |
| | 2017 | 15.7 (±1.1) | 16.4 (±0.7) | 15.9 (±0) | 15.8 (±0.6) | 15.2 (±0.6) | 15.6 (±0.4) | 15.6 (±0) | 16.1 (±0.8) |
| | $\overline{X}$ | 15.9 | 16.6 | 16.1 | 16.2 | 15.4 | 15.9 | 15.8 | 16.4 |
| $CROP_3$ | 2012 | 15.2 (±1.4) | 16.8 (±0.8) | 16.1 (±0.6) | 15.9 (±1.0) | 13.1 (±1.2) | 15.7 (±1.1) | 16.8 (±0.3) | 16.2 (±1.4) |
| | 2016 | 15.3 (±1.5) | 16.8 (±0.9) | 16.0 (±1.1) | 15.8 (±1.1) | 13.0 (±1.1) | 15.6 (±1.2) | 16.7 (±0.4) | 16.2 (±1.5) |
| | 2017 | 15.2 (±1.7) | 17.1 (±1.1) | 16.2 (±1.8) | 15.8 (±1.3) | 12.9 (±1.2) | 15.7 (±1.4) | 17.0 (±0.3) | 16.3 (±1.7) |
| | $\overline{X}$ | 15.3 | 16.9 | 16.1 | 15.9 | 13.0 | 15.6 | 16.8 | 16.2 |
| Watershed | 2012 | 15.4 (±1.3) | 16.6 (±1.0) | 15.3 (±1.1) | 15.4 (±1.1) | 12.3 (±3.4) | 15.6 (±1.1) | 15.8 (±1.8) | 15.9 (±1.5) |
| | 2016 | 15.3 (±1.4) | 16.6 (±1.1) | 15.2 (±1.3) | 15.3 (±1.3) | 12.1 (±3.5) | 15.5 (±1.2) | 15.7 (±1.8) | 15.9 (±1.6) |
| | 2017 | 15.0 (±1.5) | 16.5 (±1.2) | 14.8 (±1.3) | 14.9 (±1.4) | 11.9 (±3.4) | 15.2 (±1.3) | 15.4 (±2.0) | 15.6 (±1.7) |
| | $\overline{X}$ | 15.2 | 16.6 | 15.1 | 15.2 | 12.1 | 15.4 | 15.6 | 15.8 |